ADVANCED PHOTONICS RESEARCH
Open Access
www.adpr-journal.com

Silicon-Rich Nitride Refractive Index as a Degree of Freedom to Maximize Nonlinear Wave Mixing in Nanowaveguides

Dmitrii Belogolovskii, Nikola Alic, Andrew Grieco, and Yeshaiahu Fainman*

Silicon nitride is widely used in integrated photonics for optical nonlinear wave mixing due to its low optical losses combined with relatively high nonlinear optical properties and a wide-range transparency window. It is known that a higher concentration of Si in silicon-rich nitride (SRN) magnifies both the nonlinear response and optical losses, including nonlinear losses. To address the trade-off, four-wave mixing (FWM) is implemented in over a hundred SRN waveguides prepared by plasma-enhanced chemical vapor deposition in a wide range of SRN refractive indices varying between 2.5 and 3.2 (measured in the C-band). It is determined that SRN with a refractive index of about 3 maximizes the FWM efficiency for continuous-wave operation, indicating that the refractive index of SRN is indeed a crucial optimization parameter for nonlinear optics applications. The FWM efficiency is limited by large nonlinear optical losses observed in SRN waveguides with indices larger than 2.7, which are not related to two-photon absorption. Finally, the third-order susceptibility χ_3 and the nonlinear refractive index n_2 are estimated for multiple SRN refractive indices, and, specifically, the nonlinearities as large as $\chi_3 = (12.6 \pm 1.4) \times 10^{-19}\ m^2\ V^{-2}$ and $n_2 = (7.6 \pm 0.8) \times 10^{-17}\ m^2\ W^{-1}$ are estimated in a waveguide with an SRN refractive index of 3.2.

1. Introduction

Silicon nitride (Si_xN_y) on insulator grown by plasma-enhanced chemical vapor deposition (PECVD) is of great interest as a complementary metal-oxide semiconductor (CMOS) compatible integrated photonics platform. Indeed, the benefits of stoichiometric Si_3N_4 include very low optical losses ($<1\ dB\ cm^{-1}$),[1–3] absence of two-photon absorption (TPA) in the telecommunication spectral band,[4–6] and a broad optical transparency window.[7] Furthermore, Si_3N_4 possesses a high optical damage threshold that is well suited for high power applications,[8] enabling efficient optical nonlinear devices such as broadband nonlinear wave mixers, optical switches, modulators, and others. Even though the material is amorphous, second-order nonlinear effects have been observed in Si_3N_4 caused by surface nonlinearities due to symmetry breaking of a bulk material,[9] bulk nonlinearities,[10] and a coherent photogalvanic effect.[11] Unsurprisingly, there has been a growing number of successful demonstrations of Si_3N_4-based nonlinear devices, such as second-harmonic generation (SHG) in resonant gratings and ring resonators,[12,13] SHG in an electrically poled waveguide,[14] photoinduced SHG due a to photogalvanic effect,[15–20] coherent supercontinuum generation,[21] four-wave mixing (FWM),[22] comb generation,[23] difference frequency generation,[24] electric-field poled microresonator modulator,[25] and others.

On the other hand, Si_3N_4 has a significant advantage over the c-Si on insulator platform (SOI) in some applications because c-Si suffers from large TPA in the C-band, free-carrier absorption, a smaller transparency window starting at a wavelength of 1.2 μm, and no second-order nonlinear susceptibility χ_2.[26] However, Si_3N_4 has a much lower third-order nonlinear susceptibility χ_3,[20,27] as well as lower refractive index difference between the waveguide core and SiO_2 cladding, resulting in a lower mode-waveguide core overlap and larger effective mode area, leading to lower efficiency of nonlinear wave mixing processes. To mitigate these drawbacks, it has been reported that increasing Si concentration in silicon-rich nitride (SRN) leads to a higher refractive index and the corresponding nonlinearities. Indeed, some efficient SRN nonlinear processes, such as FWM,[28] supercontinuum generation,[29] intermodal frequency generation,[30] strong DC Kerr effect,[31] and many others, have been demonstrated to date. However, in addition to the desirable increase in the nonlinear response, the increase in Si concentration also leads to the increase in optical losses and TPA in SRN,[4,28] which obviously requires a careful material design trade-off. Notably, a reduction in optical losses has been accomplished by depositing low-pressure CVD SRN instead,[1,2] but it requires much higher temperature of deposition, which makes it incompatible with CMOS processing. An alternative approach is to use the SiD_4 precursor gas instead of SiH_4, which leads to a

D. Belogolovskii, N. Alic, A. Grieco, Y. Fainman
University of California, San Diego
9500 Gilman Drive, La Jolla, CA 92093, USA
E-mail: dbelogol@ucsd.edu

The ORCID identification number(s) for the author(s) of this article can be found under https://doi.org/10.1002/adpr.202400017.

DOI: 10.1002/adpr.202400017

reduction of optical losses in an SRN waveguide due to the absence of Si—H and N—H bonds in C-band, but the SiD_4 gas is not always available.[1,32,33] It is also possible to optimize a PECVD recipe by varying high frequency to lower frequency RF power ratio to break hydrogen bonds and reduce optical losses,[34] but it may also alter other optical parameters. Overall, an SRN refractive index becomes an important degree of freedom for nonlinear mixing device efficiency optimization.

In this article, we experimentally investigate a wide-range (varying between 2.5 and 3.2) SRN refractive index effect on the nonlinear mixing efficiency in the C-band. Furthermore, we use FWM efficiency to retrieve the material χ_3 for each of the SRN samples, as well as to identify the optimal device SRN refractive index in terms of nonlinear efficiency optimization. Specifically, the characterization included the effects of both linear and nonlinear optical losses on the FWM efficiency, which have been determined as a function of waveguide geometry and optical power, respectively. While FWM in SRN waveguides was implemented previously, it was almost universally demonstrated for only a single SRN refractive index in each published study, for different wavelengths or SRN deposition recipes, making the comparison between different results from published studies rather difficult. This work, however, provides a comprehensive rigorous study of the SRN platform in which the samples with widely ranging parameters were fabricated in the same controlled conditions, including the same fabrication flow and equipment, thus allowing a proper systematic comparison between a large number of samples made of SRN films with different refractive indices. Finally, we also provide a novel report on the observation of nonlinear optical losses in high index PECVD SRN waveguides not caused by TPA, and how such losses affect the efficiency of FWM at higher power. Thus, the novel results of this study have important design ramifications for researchers working on SRN-based components and devices.

The article is organized as follows: The fundamentals of the underlying theory and methodology are contained in Section 2, samples fabrication and the characterization are described in Section 3, and the experimental results are detailed in Section 4. Finally, the findings and conclusions of this study are summarized and discussed in Section 5.

2. Degenerate FWM Theory

The efficiency of degenerate FWM in a waveguide under the assumption of undepleted pump approximation and absence of nonlinear losses can be described by[35]

$$\mu = \frac{P_i}{P_s} = |\gamma P_p L_{\text{eff}}|^2 \tag{1}$$

where

$$\gamma = \frac{\omega n_2}{c A_{\text{eff}}} = \frac{3\omega\chi_3}{4\varepsilon_0 c^2 A_{\text{eff}} n_{\text{eff}}^2} \tag{2}$$

$$L_{\text{eff}}^2 = L^2 \exp\ (-\alpha L)\left|\frac{1-\exp\ (-\alpha L - i\Delta k L)}{\alpha L + i\Delta k L}\right|^2 \tag{3}$$

$$k = 2k_p - k_i - k_s \tag{4}$$

$$k_j = \frac{2\pi n_{\text{eff},j}}{\lambda_j}, \quad j = i, p, s \tag{5}$$

$$\Gamma = \frac{\left|\iint_A \chi_3 E^4\, \mathrm{d}x\, \mathrm{d}y\right|^2}{\iint_{-\infty}^{+\infty} |\chi_3 E^3|^2\, \mathrm{d}x\, \mathrm{d}y \iint_{-\infty}^{+\infty} |E|^2\, \mathrm{d}x\, \mathrm{d}y} \tag{6}$$

where indices i, p, and s represent the idler, pump, and signal, P_j is the optical power, γ is a nonlinear effective coefficient, n_2 is a nonlinear refractive index, ω is the optical frequency of pump, χ_3 is the third-order nonlinear susceptibility, ε_0 is the vacuum permittivity, c is the speed of light, A_{eff} is the effective mode area, n_{eff} is the modal effective index, α is the optical loss coefficient, L is the waveguide length, k_j is the wave vector, k is the mode phase mismatch, λ_j is the wavelength, Γ stands for the modal overlap integral, A represents an SRN integration area limited by the core width and height, and E is the mode electric field in the transverse plane. We ignore the SiO_2 cladding contribution to FWM in SRN waveguides because χ_3 of SiO_2 is much smaller than that of SRN used in our study even for the lowest SRN refractive index.

As follows from the FWM efficiency given by Equation (1)–(6), the increase in the mixing efficiency requires some combination of lower optical losses, increase in χ_3 and mode confinement in the waveguide, or, conversely, decrease the effective mode area and dispersion. In waveguides with nonzero dispersion and considerable loss, the FWM efficiency is generally governed by the relevant characteristic lengths: the maximum length due to optical losses $L_{\text{loss}} \approx 1/\alpha$, or a coherence length $L_{\text{coh}} = \pi/k$. As it will be shown later in the article, in the setup used in our measurements, the losses were the limiting factor, imposing a limit on the devices' length of a few millimeters, while the dispersion set a limit on the scale of centimeters for the chosen wavelengths for the pump, signal, and idler. Therefore, in our case the FWM efficiency can be most appropriately expressed as follows:

$$\mu \approx \left(\frac{\chi_3}{\alpha A_{\text{eff}} n_{\text{eff}}^2}\right)^2 \tag{7}$$

showing the equivalent importance of χ_3 and optical losses. Additionally, we would also like to point out that the reduction in the effective area may be equally important in this respect, which can be achieved in waveguides with a high SRN refractive index.

3. Experimental Design and Sample Fabrication

To facilitate the wide-ranging characterization, over a hundred waveguides were fabricated having four different lengths (0.3, 2.4, 4.4, and 6.5 mm), with refractive indices in the range of 2.5–3.2 and with varying waveguide widths. To fabricate our samples, we used SOI wafers with a 3 μm buried oxide (BOX) layer and a 220 nm Si device layer, which was removed by tetramethylammonium hydroxide wet etching (note that this step can be avoided if Si wafers with only a SiO_2 layer on the top are available). Then, an SRN thin film was deposited in a Plasmalab PECVD, with a stage temperature set to 350 °C, while using SiH_4 and N_2 precursor gases. The ratio of gases was varied to change the refractive index of the SRN thin films, as shown

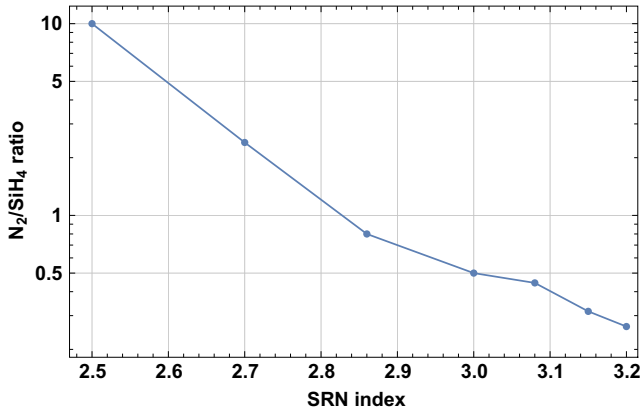

Figure 1. N_2/SiH_4 gas ratio utilized to deposit PECVD SRN films with a corresponding refractive index measured at 1550 nm.

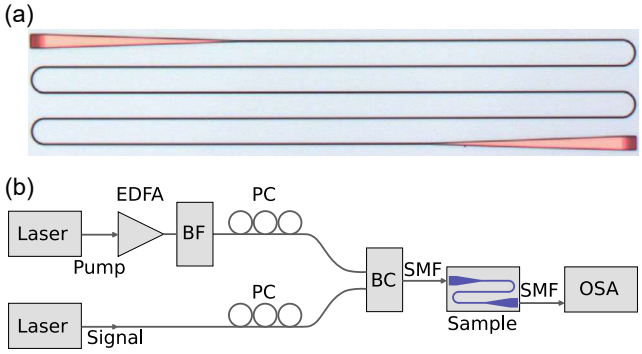

Figure 2. a) Optical microscope image of a typical SRN waveguide fabricated in a serpentine shape for a compact design. b) Block diagram of the experimental apparatus used to perform FWM in SRN waveguides and its characterization. EDFA, erbium-doped fiber amplifier; BP, bandpass filter; PC, polarization controller; BC, 3 dB beam combiner; SMF, single-mode fiber coupler; OSA, optical spectrum analyzer.

in **Figure 1**. The thin film thickness and refractive index were measured by a J.A. Woollam M-2000D ellipsometer. Next, the hydrogen silsesquioxane (HSQ) e-beam resist was spun on the sample, before being patterned by e-beam lithography. After being developed, the sample was etched in a Plasmalab P100, and HSQ was removed by 6:1 buffered oxide etch. The final step consisted of depositing a SiO_2 cladding in a Plasmalab PECVD.

The light coupling in and out of the waveguides was enabled by fully etched linearly apodized grating couplers (GCs) with long 300 μm tapers. Coupling efficiency (CE) maximization was enabled by simulations in Ansys (Lumerical), including calculations of GC-optimal parameters such as the filling factor, linear apodization factor, and others.[36] Unlike edge couplers that require dicing, which adds an extra step of fabrication, fully etched GC can be done in one step of e-beam lithography along with waveguides, simplifying the fabrication flow. Additionally, in our practice edge couplers suffered from significant edge roughness caused by dicing in our facility, which led to relatively low CE of −10 dB per edge coupler. Therefore, the Bosch process was necessary to deep etch the edges to make them smoother, which would increase CE, but also would complicate the fabrication flow, which must have been avoided because many samples needed to be fabricated. At the same time, GCs were found quite efficient, yielding CE as high as −4.5 dB per GC, while −3 dB was a theoretical maximum due to a symmetry of the fully etched GC. They had a spectral bandwidth of 40 nm, large enough to efficiently couple in and out the pump, signal, and idler with a wavelength gap of 5 nm. We used single-mode (SM) fibers to couple light in and out of a sample as unlike tapered fibers, they can handle higher power without optical damage.

To measure the FWM-generated idler, we combined the pump and the signal (both operated in the continuous wave (CW) regime) and coupled them to an SRN waveguide, which is shown in **Figure 2**a as an optical microscope image. A C-band tunable narrowband (≈100 kHz) Agilent 81980A laser was used as a signal source, while a tunable narrowband (≈100 kHz) Agilent 81642A laser amplified by an IPG Photonics EAD-3-C erbium-doped fiber amplifier (EDFA) was used as a pump source. The EDFA noise was removed by a bandpass filter. Polarization controllers (PC) were used to set the waves' polarization to the transverse electric (TE) state. The signal and pump were combined through a beam combiner (BC) and coupled to a sample under test. The generated idler together with the residual pump and signal was coupled out and measured by a Yokogawa AQ6375 optical spectrum analyzer (OSA). The setup block diagram is shown in Figure 2b.

The wavelength difference between the pump and the signal was set to 5 nm, large enough to avoid suppression of the small-power idler by the high-power pump caused by a dynamic range limit of the OSA, while small enough to avoid phase mismatch caused by the dispersion in a long waveguide and fit within the spectral bandwidth of the GC. The negligible level of FWM in the silica patch cords used was independently verified by removing the SRN sample from the setup, whereby no idler was distinguishable on the OSA above the −67 dBm noise level, matching the theoretical estimation.

A waveguide geometry for all samples was chosen such that each SRN index waveguide remained SM to avoid high-order mode interference while maintaining the mode overlap integral Γ approximately constant (≈0.5) for each SRN sample considered. In particular, to satisfy the latter condition, the thickness of the waveguides was maintained around 350 nm, while the corresponding widths varied from 375 nm (for the index of 3.2) to 550 nm (for the index 2.5). The BOX layer was maintained at 3 μm and the top cladding at 1 μm for all samples. **Table 1** summarizes the SRN waveguide parameters simulated in Lumerical (Ansys) for different SRN refractive indices and geometry, where n is the SRN refractive index, w is the waveguide core width, d is the waveguide core thickness, A_{eff} is the effective mode area, n_{eff} is the effective index of a SRN waveguide, and Γ is the overlap integral defined by Equation (6).

4. Results

4.1. FWM

With the objective of determining the most optimal refractive index of SRN for FWM, we fabricated more than a hundred

Table 1. Waveguide parameters retrieved from Lumerical (Ansys) simulations based on an SRN index and waveguide core geometry for a TE mode.

n	w [nm]	d [nm]	A_{eff} [μm^2]	n_{eff}	Γ
2.5	550	383	0.43	1.87	0.49
2.7	500	386	0.36	2	0.51
2.86	480	390	0.32	2.13	0.54
2.96	400	377	0.32	2.06	0.43
3	440	337	0.29	2.13	0.5
3.08	424	351	0.28	2.2	0.51
3.15	375	343	0.28	2.13	0.42
3.2	375	337	0.27	2.17	0.45

SRN devices with different refractive indices and waveguide lengths and captured the corresponding spectra on the OSA with a typical example (for a refractive index of 3.15) shown in **Figure 3**a. Based on the generated idler power and GC CE, we calculated the idler power on a chip at the end of a waveguide, and the pump power and signal power at the beginning of a waveguide. Based on Equation (1)–(6), the FWM efficiency of each device was calculated for each waveguide length. The maximum efficiency was then retrieved from the FWM efficiency dependence on a waveguide length by fitting, as illustrated in Figure 3b for an SRN waveguide sample having a refractive index of 3.15.

Considering that the shortest waveguide length was approximately the same as that of the tapers (300 μm), it was important to calculate the FWM in the tapers as well. For that, the taper was split into small sections, and the parameters such as shown in Table 1 were calculated for each section. Then, the idler generation in each section was calculated based on Equation (1)–(6). The total power of the idler generated in the two tapers was approximately the same as that in a 300 μm SRN waveguide. Consequently, the SRN FWM efficiencies throughout the article have been rigorously presented by subtracting FWM powers generated by tapers.

Figure 4a summarizes the measurements of the FWM efficiency μ, where its dependence on an SRN index of refraction is presented. As it can be seen in Figure 4a, the efficiency steadily grows starting with a refractive index of 2.5 and peaks for the value of 2.96. Further increase in the index lowers the efficiency due to higher optical losses, even though χ_3 continues to increase. It is also important to note that in waveguides with indices greater than 2.7 FWM efficiency increases slower than P_p^2, indicating the presence of nonlinear losses. The latter effect is

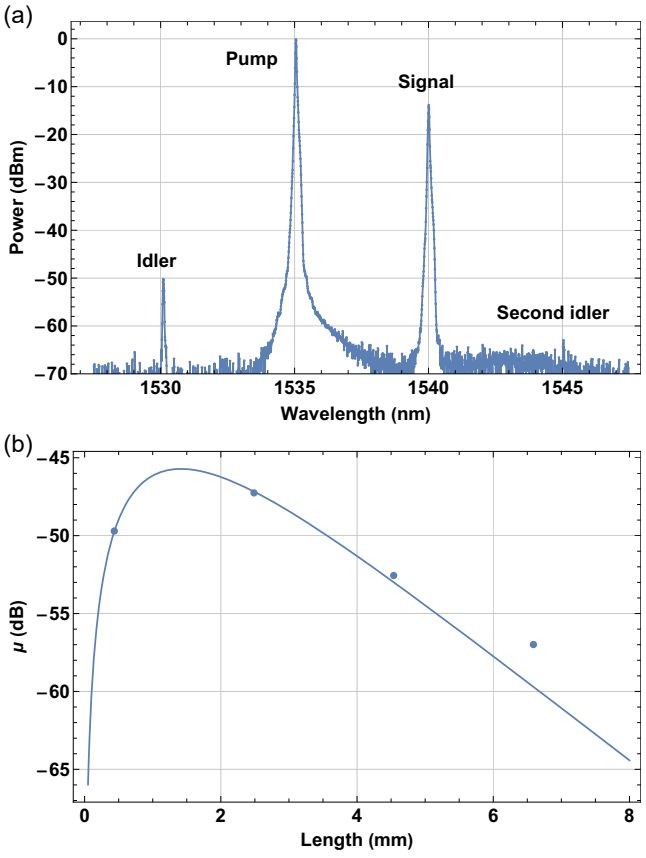

Figure 3. FWM implemented in a 3.15 SRN index waveguide at on-chip pump power of about 40 mW: a) FWM spectrum measured by the OSA and b) FWM efficiency dependence on a waveguide length.

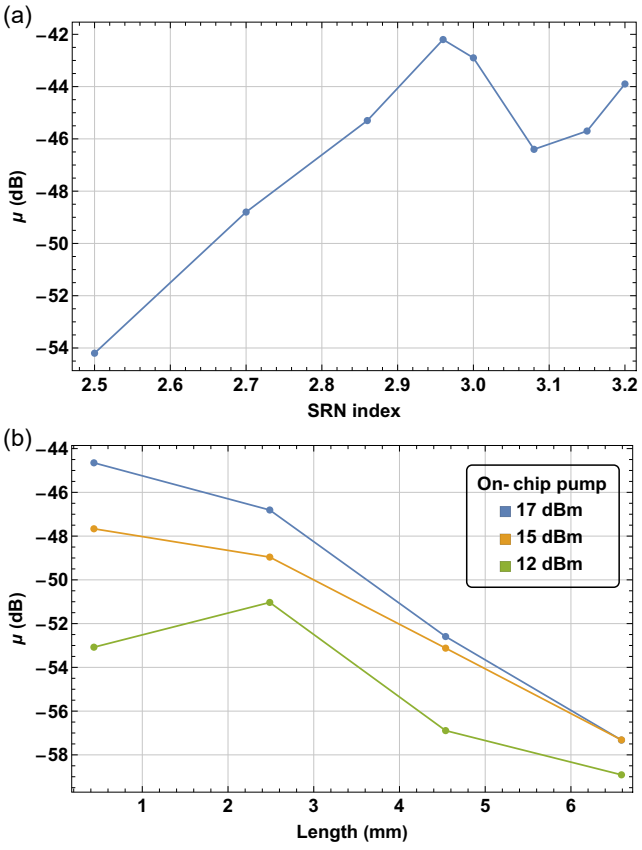

Figure 4. a) FWM efficiency as a function of an SRN index. b) FWM in a 3.2 SRN index waveguide as a function of on-chip pump power for four different lengths.

exemplified in Figure 4b for the SRN sample refractive index of 3.2 SRN waveguides.

As implied by the results shown in Figure 4b, in the shortest waveguide (300 μm) the pump power reduction from 17 to 12 dBm leads to a 10 dB of efficiency decrease, which follows the expected P_p^2 dependence. However, in longer waveguides (2.3–6.5 mm) this is no longer the case. For example, a 5 dBm of pump power reduction in the longest waveguide of 6.5 mm leads to only 2 dB of efficiency decrease, indicating strong nonlinear losses in this case. Hence, it is anticipated that if pump power continues to increase, the peak of FWM efficiency from Figure 4a will shift to a lower index due to higher nonlinear optical losses in a larger index of SRN. Note that these experiments are valid for CW optical fields operation. As it will be shown later, the nonlinear losses are not related to TPA.

Based on the calculated FWM efficiency and theoretical Equation (1)–(6), the sample's χ_3 was extracted as a function of an SRN index that was fitted by a curve described by the Miller's $\chi_3 \approx \chi_1^4$ rule, both results are shown in **Figure 5**a. As shown in Figure 5a, the measured χ_3 generally follows the Miller's rule well, only slightly deviating from it at lower SRN indices (those lower than 2.7). The maximum $\chi_3 = (12.6 \pm 1.4) \times 10^{-19}\,\mathrm{m^2\,V^{-2}}$ was estimated for the 3.2 index, while the minimum one of $\chi_3 = (1.56 \pm 0.17) \times 10^{-19}\,\mathrm{m^2\,V^{-2}}$ corresponded to the 2.5 index, which is about 8 times lower. As a countercheck, we also measured $\chi_3 = (3.3 \pm 0.4) \times 10^{-19}\,\mathrm{m^2\,V^{-2}}$ in a c-Si waveguide by the exact same method as for SRN waveguides, shown in Figure 5a as a separate point. The obtained parameter from the c-Si tests agrees very well with other reported results for the same material,[26] indirectly confirming the validity of our SRN measurements. Notably, the χ_3 value for the index 3.2 is almost 4 times as large as that of c-Si.

Finally, the n_2 dependence on the refractive index is shown in Figure 5b. The waveguide parameters, including the effective indices, were taken from Table 1. As it can been seen in Figure 5b, the trend is similar to that for the χ_3 as expected based on Equation (2), showing that $n_2 = (1.26 \pm 0.14) \times 10^{-17}\,\mathrm{m^2\,W^{-1}}$ for the lowest 2.5 SRN index, while it is $n_2 = (7.6 \pm 0.8) \times 10^{-17}\,\mathrm{m^2\,W^{-1}}$ for the largest 3.2 SRN index. Here, we also provide **Table 2** that presents n_2 or χ_3 measured by different research groups by various methods, such as z-scan, FWM, DC Kerr effect, or self-phase modulation (SPM), and compare them with some of our results.[6,28,31,37]

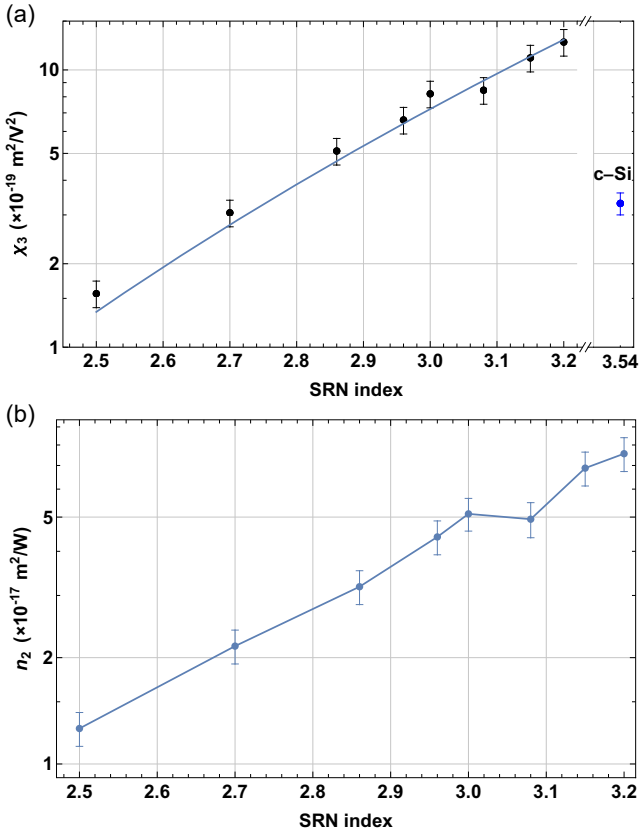

Figure 5. a) Estimated χ_3 as a function of a SRN index (black dots) fitted by the Miller's rule curve (blue curve) and estimated χ_3 of c-Si. b) n_2 dependence on SRN index. The fitting curve was retrieved from Wolfram Mathematica; the error bars represent the standard deviation error based on three to five measurements per an SRN index.

4.2. Optical Losses in SRN Waveguides

In this subsection, we shall examine in more detail the observed sharp drop of the FWM efficiency for SRN samples having a refractive index higher than 2.96. Specifically, we measured an optical loss coefficient at both low and high powers using the cutback method. First, with the objective of avoiding nonlinear losses, light transmission was measured in each waveguide at low on-chip power of 500 μW, whereas optical losses were calculated based on the light transmission change as a function of a waveguide length, as shown in **Figure 6**a. An optical loss coefficient as a function of an SRN waveguide index and core width is shown in Figure 6b.

As is apparent from Figure 6b, optical losses in the low-power (i.e., linear) regime increase with a higher SRN index and a smaller waveguide core width, a result that is consistent with previous research reports on the subject.[28] Here, we note that it is widely accepted in the literature that optical losses are predominantly caused by Si—H and N—H bonds in SRN films, as well as scattering due to surface roughness of sidewalls and top surface roughness of the waveguide core.[1–3,38,39] Note that chemical–mechanical polishing (CMP) can be used to smooth out the

Table 2. n_2 and χ_3 measured in various compositions of SRN in C-band by different research groups.

References	n	n_2 [$\times 10^{-17}\,\mathrm{m^2\,W^{-1}}$]	χ_3 [$\times 10^{-19}\,\mathrm{m^2\,W^{-2}}$]	Method
[37]	3.1	2.8	–	SPM
[6]	3.1	2.93	–	z-scan
[31]	3	–	6.0	DC Kerr
[28]	2.7	0.2	–	FWM
[28]	2.5	0.16	–	FWM
This work	3.1	5.0	8.5	FWM
This work	2.7	2.2	3.1	FWM
This work	2.5	1.25	1.56	FWM

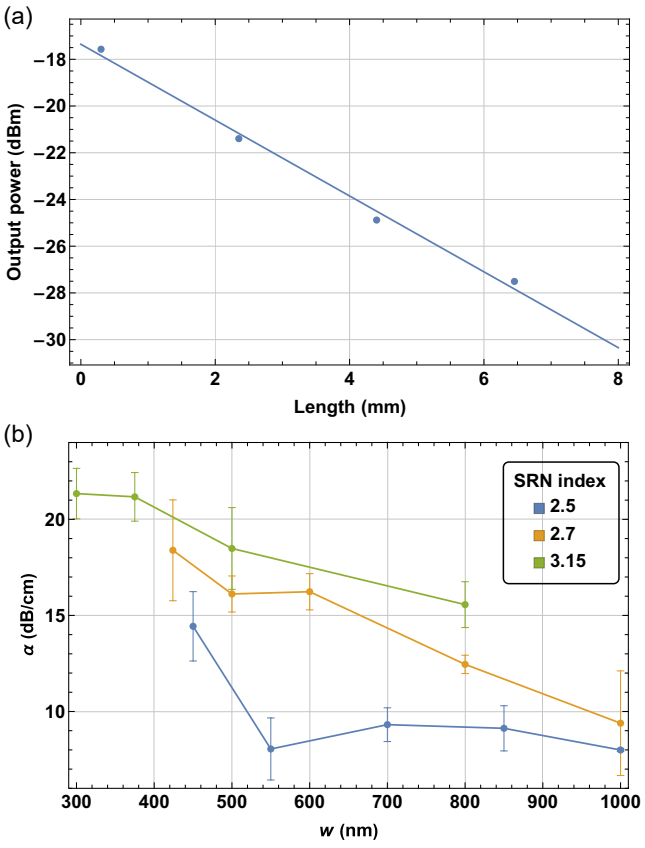

Figure 6. a) Output power as a function of a waveguide length in a 3.15 index SRN waveguide with a core width of 600 nm, fitted by a linear function in Wolfram Mathematica to retrieve an optical loss coefficient. b) Optical loss coefficient α as a function of a width of an SRN waveguide core w for various SRN indices, measured at low optical power for a TE mode; the error bars represent the standard deviation error from the fitting.

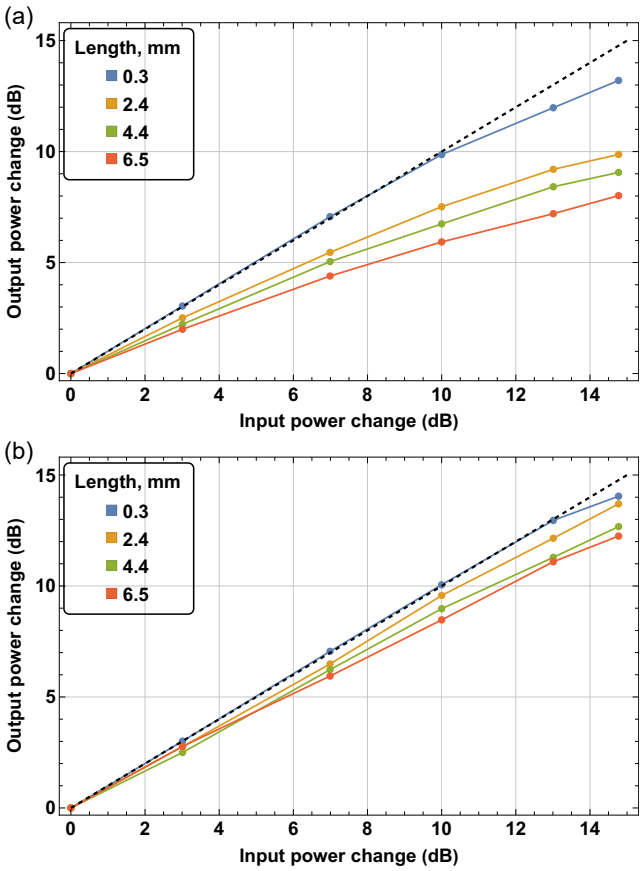

Figure 7. Measured output power increase as a function of on-chip power increase in a waveguide for an a) SRN index of 3.2 and b) SRN index of 2.7; the dashed black line indicates no nonlinear loss.

top surface roughness to reduce scattering losses,[1,3,39] although CMP was not done in our experiments because it was not available to us. Consequently, large scattering losses prevail in smaller waveguide cores due to waveguide modes being pushed out of the waveguide core, which leads to a stronger electrical field of a mode being present on the rough sidewalls of a waveguide. Although a mode is well confined in a larger waveguide, losses still remain high for a larger SRN index, which indicates that SRN material losses also increase for SRN films with a higher refractive index. Optical losses as high as 21 dB cm^{-1} were measured in a 3.15 index SRN in a SM waveguide with a 375 nm core width, while 8 dB cm^{-1} losses were measured in a 2.5 index SRN in a SM waveguide with a 550 nm core width. Overall, measured optical losses are higher in PECVD SRN waveguides than in typical c-Si waveguides.

As noted previously, optical losses also increase with an increase in the pump power in SRN waveguides for indices greater than 2.7. To observe the effect, the on-chip power was increased from about 1.5–40 mW (nearly a 15 dB increase) to measure transmission as a function of power. The results are shown in **Figure 7** for SRN indices of 2.7 and 3.2, where a measured output power change is plotted as a function of an on-chip input power change for various lengths of SRN waveguides.

Figure 6 shows that the transmission of the pump power in SRN samples having refractive indices of 2.7 and 3.2 deviates from a linear dependence (indicated by the dashed line), which suggests the presence of nonlinear losses in the material. The transmission is reduced for higher coupled power in SRN for both indices for longer waveguide lengths, indicating that the effect is caused by SRN waveguides rather than GCs, tapers, or other components in the setup. While nonlinear losses were seen in all our SRN waveguides with indices 2.7–3.2, no nonlinear losses were observed in c-Si waveguides and 2.5 index SRN waveguides. Furthermore, transmission of the signal power also reduces if high pump power is present in the same waveguide, the effect gets stronger for a larger SRN index at higher pump power in longer waveguides, similar to the pump. For instance, at pump power of 40 mW coupled to an SRN waveguide with a refractive index of 3.2 and a length of 6.5 mm, we observed extra 10 dB of signal loss. Consequently, it significantly reduces the efficiency of FWM as the pump, signal, and idler power gets reduced.

While the particular mechanism for increased nonlinear losses is not entirely understood, it does not seem to be related to TPA, as explained next (even though some previous publications reported TPA in a high index SRN[28]). Specifically, in order to examine the source of the cause of these losses, we measured

high power light transmission in the waveguides with a refractive index of 3 with core widths varying between 440 and 5000 nm. Indeed, such a large difference is necessary to reduce the peak intensity in the larger waveguides in order to minimize (or eliminate) the potential for TPA. In these measurements, the transmission in the larger waveguides did not change significantly, indicating that the nonlinear loss mechanism depends on average power rather than peak intensity, thereby precluding the occurrence of TPA. Furthermore, this result also excludes other nonlinear processes that depend on peak intensity, such as stimulated Brillouin scattering.

To better characterize the observed nonlinear losses, we introduce the nonlinear loss coefficient β in Equation (8), which follows the same equation as a TPA coefficient for a given waveguide geometry:

$$\frac{dI}{dz} = -\beta I^2 \tag{8}$$

where I is the optical intensity of a mode propagating in a z direction. Based on the results demonstrated in Figure 7, we calculated an output optical intensity as a function of an SRN waveguide length and fitted it in Wolfram Mathematica with the solution from the Equation (8) while taking into consideration an overlap integral in an SRN waveguide core. The result is shown in **Figure 8**a for an SRN index of 3.2. From the fitting we estimated the nonlinear coefficients of multiple indices of SRN waveguides and presented the results in Figure 8b.

It follows from Figure 8a that the loss coefficient β indeed follows a linear dependence on optical intensity assumed in Equation (8), similar to TPA. However, the estimated coefficient β is significantly higher than the TPA coefficient β_{TPA} reported in c-Si. Explicitly, $\beta_{TPA} = 0.015\,\mathrm{m\,GW^{-1}}$ in c-Si in the C-band is ≈2 orders of magnitude lower than $\beta = (1.82 \pm 0.17)\,\mathrm{m\,GW^{-1}}$ estimated for the 2.7 index SRN waveguide in our measurements.[26] Furthermore, it is important to note that unlike in the case of TPA, β depends on geometry of a waveguide. Therefore, the comparison with TPA here is only reasonable for comparable geometry of waveguides. Nevertheless, the direct comparison clearly demonstrates that SRN waveguides with a refractive index higher than 2.7 exhibit significantly higher nonlinear losses than c-Si for CW signals.

A detailed study of the nonlinear loss dynamics is beyond the scope of this article and will be published elsewhere. Suffice it to say that the effect can be reduced and even eliminated with an appropriate short-pulse excitation. As an illustration, **Figure 9** demonstrates the propagation of a pulsed 1550 nm wavelength laser source, with 200 fs pulses and 10 MHz repetition rate. The pulses were generated by an FPL-02CFTUSD12 Calmar laser.

As observed in Figure 9, even at high peak power of 5 W coupled to a 440 nm wide SRN waveguide with a refractive index of 3, no nonlinear losses can be observed, and the transmitted power follows a linear dependence on the coupled power. The last result indicates that not only is it possible to suppress the nonlinear losses with a proper excitation, but, more importantly, it also precludes the TPA as their source, even at very high peak power.

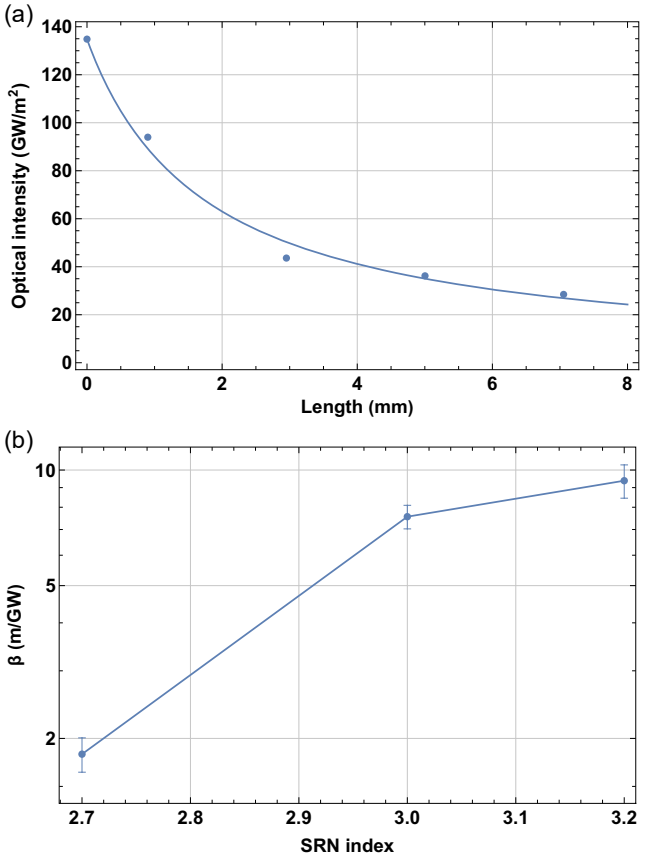

Figure 8. a) Fitted output optical intensity on chip as a function of a waveguide length for an SRN index of 3.2 at 40 mW power. b) Estimated β coefficient for different SRN indices; the error bars are retrieved from fitting in Wolfram Mathematica as the standard deviation error.

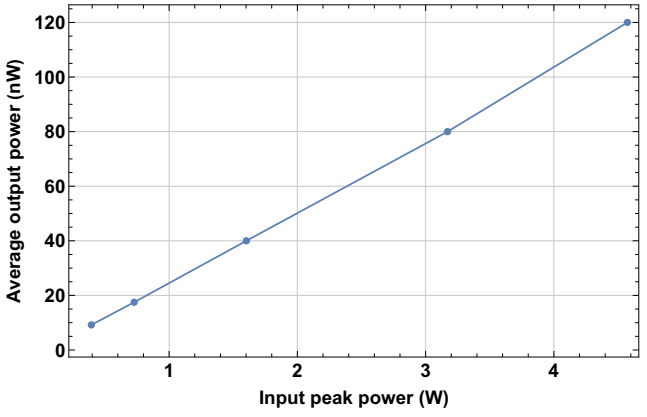

Figure 9. Measured average output power as a function of on-chip peak power in a 440 nm index 3 SRN waveguide for 200 fs pulses with a 10 MHz repetition rate.

5. Conclusion

In conclusion, we have presented a comprehensive study of the nonlinear optical properties of SRN SM waveguides. Our investigation was primarily based on FWM efficiency characterization.

Specifically, we have demonstrated that the refractive index in SRN waveguides represents an important degree of freedom that can be used to optimize the nonlinear wave mixing. Most importantly, novel results have revealed the existence of a trade-off between the nonlinear response of SRN and optical losses, including nonlinear losses at higher power. In fact, a refractive index of around 3 (at 1550 nm) of SRN waveguides maximized the efficiency of FWM for CW operation in the C-band. On top of that, we have measured the maximum $n_2 = (7.6 \pm 0.8) \times 10^{-17}\,\mathrm{m^2\,W^{-1}}$ and $\chi_3 = (12.6 \pm 1.4) \times 10^{-19}\,\mathrm{m^2\,V^{-2}}$ in a refractive index 3.2 SRN waveguide, which is almost 4 times larger than that in c-Si. However, it was also observed that an SRN waveguide with a refractive index of 3.2 suffers from higher optical losses, limiting the maximum useful length of an SRN waveguide device. The optical losses, caused by both sidewalls scattering and an SRN waveguide core absorption, can be reduced by increasing a waveguide core thus minimizing scattering losses. We have also observed and characterized nonlinear optical losses in SRN waveguides (with a refractive index higher than 2.7) at higher CW power, and we have shown that the nonlinear losses are not related to TPA as it is possible to altogether eliminate the nonlinear losses by utilizing high peak power short pulses (200 fs).

Thus, we have established the importance of measuring optical losses at high CW optical power in order to optimize an SRN fabrication recipe and ensure the optimal operation of nonlinear devices in this platform due to the existence of nonlinear losses.

Acknowledgements

The authors thank SDNI and all UCSD's nano3 cleanroom staff and Dr Maribel Montero for their assistance with samples fabrication.

Conflict of Interest

The authors declare no conflict of interest.

Author Contributions

All authors have accepted responsibility for the entire content of this manuscript and approved its submission.

Data Availability Statement

The datasets generated during and/or analyzed during the current study are available from the corresponding author on reasonable request.

Keywords

integrated photonics, nonlinear optical losses, nonlinear optics, silicon nitride, silicon photonics

Received: February 1, 2024
Revised: May 6, 2024
Published online: May 22, 2024

[1] A. Frigg, A. Boes, G. Ren, I. Abdo, D.-Y. Choi, S. Gees, A. Mitchell, *Opt. Express* **2019**, *27*, 37795.
[2] J. F. Bauters, M. J. R. Heck, D. John, D. Dai, M.-C. Tien, J. S. Barton, A. Leinse, R. G. Heideman, D. J. Blumenthal, J. E. Bowers, *Opt. Express* **2011**, *19*, 3163.
[3] X. Ji, F. A. S. Barbosa, S. P. Roberts, A. Dutt, J. Cardenas, Y. Okawachi, A. Bryant, A. L. Gaeta, M. Lipson, *Optica* **2017**, *4*, 619.
[4] K. J. A. Ooi, D. K. T. Ng, T. Wang, A. K. L. Chee, S. K. Ng, Q. Wang, L. K. Ang, A. M. Agarwal, L. C. Kimerling, D. T. H. Tan, *Nat. Commun.* **2017**, *8*, 13878.
[5] D. T. H. Tan, K. J. A. Ooi, D. K. T. Ng, *Photonics Res.* **2018**, *6*, B50.
[6] B.-U. Sohn, J. W. Choi, D. K. T. Ng, D. T. H. Tan, *Sci. Rep.* **2019**, *9*, 10364.
[7] R. Soref, *Nat. Photonics* **2010**, *4*, 495.
[8] L. Zhang, Y. Li, Y. Hou, Y. Wang, M. Tao, B. Chen, Q. Na, Y. Li, Z. Zhi, X. Liu, X. Li, F. Gao, X. Luo, G.-Q. Lo, J. Song, *Opt. Express* **2021**, *29*, 29755.
[9] Y. R. Shen, *Nature* **1989**, *337*, 519.
[10] M. W. Puckett, R. Sharma, H.-H. Lin, M. Han Yang, F. Vallini, Y. Fainman, *Opt. Express* **2016**, *24*, 16923.
[11] M. A. Porcel, J. Mak, C. Taballione, V. K. Schermerhorn, J. P. Epping, P. J. van der Slot, K.-J. Boller, *Opt. Express* **2017**, *25*, 33143.
[12] T. Ning, H. Pietarinen, O. Hyvärinen, R. Kumar, T. Kaplas, M. Kauranen, G. Genty, *Opt. Lett.* **2012**, *37*, 4269.
[13] J. S. Levy, M. A. Foster, A. L. Gaeta, M. Lipson, *Opt. Express* **2011**, *19*, 11415.
[14] Y. Zhang, J. Nauriyal, M. Song, M. G. Baez, X. He, T. Macdonald, J. Cardenas, *Opt. Mater. Express* **2023**, *13*, 237.
[15] D. D. Hickstein, D. R. Carlson, H. Mundoor, J. B. Khurgin, K. Srinivasan, D. Westly, A. Kowligy, I. I. Smalyukh, S. A. Diddams, S. B. Papp, *Nat. Photonics* **2019**, *13*, 494.
[16] E. Nitiss, O. Yakar, A. Stroganov, C.-S. Brès, *Opt. Lett.* **2020**, *45*, 1958.
[17] E. Nitiss, T. Liu, D. Grassani, M. Pfeiffer, T. J. Kippenberg, C.-S. Brès, *ACS Photonics* **2020**, *7*, 147.
[18] D. Grassani, M. H. P. Pfeiffer, T. J. Kippenberg, C.-S. Brès, *Opt. Lett.* **2019**, *44*, 106.
[19] X. Lu, G. Moille, A. Rao, D. A. Westly, K. Srinivasan, *Nat. Photonics* **2021**, *15*, 131.
[20] A. Billat, D. Grassani, M. H. P. Pfeiffer, S. Kharitonov, T. J. Kippenberg, C.-S. Brès, *Nat. Commun.* **2017**, *8*, 1016.
[21] A. R. Johnson, A. S. Mayer, A. Klenner, K. Luke, E. S. Lamb, M. R. E. Lamont, C. Joshi, Y. Okawachi, F. W. Wise, M. Lipson, U. Keller, A. L. Gaeta, *Opt. Lett.* **2015**, *40*, 5117.
[22] M. Ferrera, D. Duchesne, L. Razzari, M. Peccianti, R. Morandotti, P. Cheben, S. Janz, D.-X. Xu, B. E. Little, S. Chu, D. J. Moss, *Opt. Express* **2009**, *17*, 14098.
[23] K. Luke, Y. Okawachi, M. R. E. Lamont, A. L. Gaeta, M. Lipson, *Opt. Lett.* **2015**, *40*, 4823.
[24] E. Sahin, B. Zabelich, O. Yakar, E. Nitiss, J. Liu, R. N. Wang, T. J. Kippenberg, C.-S. Brès, *Nanophotonics* **2021**, *10*, 1923.
[25] B. Zabelich, C. Lafforgue, E. Nitiss, A. Stroganov, C.-S. Brès, *APL Photonics* **2024**, *9*, 016101.
[26] N. K. Hon, R. Soref, B. Jalali, *J. Appl. Phys.* **2011**, *110*, 011301.
[27] K. Ikeda, R. E. Saperstein, N. Alic, Y. Fainman, *Opt. Express* **2008**, *16*, 12987.
[28] C. Lacava, S. Stankovic, A. Z. Khokhar, T. D. Bucio, F. Y. Gardes, G. T. Reed, D. J. Richardson, P. Petropoulos, *Sci. Rep.* **2017**, *7*, 22.
[29] Y. Cao, B.-U. Sohn, H. Gao, P. Xing, G. F. R. Chen, D. K. T. Ng, D. T. H. Tan, *Sci. Rep.* **2022**, *12*, 9487.
[30] C. Lacava, T. D. Bucio, A. Z. Khokhar, P. Horak, Y. Jung, F. Y. Gardes, D. J. Richardson, P. Petropoulos, F. Parmigiani, *Photonics Res.* **2019**, *7*, 615.

[31] A. Friedman, H. Nejadriahi, R. Sharma, Y. Fainman, *Opt. Lett.* **2021**, *46*, 4236.
[32] X. X. Chia, G. F. R. Chen, Y. Cao, P. Xing, H. Gao, D. K. T. Ng, D. T. H. Tan, *Sci. Rep.* **2022**, *12*, 12697.
[33] X. X. Chia, D. T. H. Tan, *Nanophotonics* **2023**, *12*, 1613.
[34] H. Kim, J. Aziz, V. D. Chavan, D. Kee Kim, *Curr. Appl. Phys.* **2024**, *57*, 59.
[35] F. Martini, A. Politi, *Appl. Phys. Lett.* **2018**, *112*, 251110.
[36] R. Marchetti, C. Lacava, A. Khokhar, X. Chen, I. Cristiani, D. J. Richardson, G. T. Reed, P. Petropoulos, P. Minzioni, *Sci. Rep.* **2017**, *7*, 16670.
[37] T. Wang, D. K. T. Ng, S.-K. Ng, Y.-T. Toh, A. K. L. Chee, G. F. R. Chen, Q. Wang, D. T. H. Tan, *Laser Photonics Rev.* **2015**, *9*, 498.
[38] E. A. Douglas, P. Mahony, A. Starbuck, A. Pomerene, D. C. Trotter, C. T. DeRose, *Opt. Mater. Express* **2016**, *6*, 2892.
[39] S. C. Mao, S. H. Tao, Y. L. Xu, X. W. Sun, M. B. Yu, G. Q. Lo, D. L. Kwong, *Opt. Express* **2008**, *16*, 20809.